Accurate and General Solutions to Three-Dimensional Anisotropies: Applications to EPR Spectra of Triplets Involving Dipole−Dipole, Spin−Orbit Interactions and Liquid Crystals

Qixi Mi, Mark A. Ratner,* and Michael R. Wasielewski*

Department of Chemistry and Argonne-Northwestern Solar Energy Research (ANSER) Center, Northwestern University, Evanston, Illinois 60208-3113

Received: April 23, 2010; Revised Manuscript Received: June 30, 2010

Thanks to the squared Cartesian coordinates and its corresponding ternary diagram, several types of anisotropic physical quantities are expressed by a weighted mean of their principal values. Specifically, in terms of the electron paramagnetic resonance (EPR) spectra of triplet states under various conditions, the anisotropies in the resonance field (due to spin dipole−dipole interaction), in the spin polarization (due to spin−orbit intersystem crossing, SO-ISC), and in the distribution of molecular orientations (due to liquid crystal alignment) are all linearized. The spectral intensity becomes a path integral on the ternary diagram along the field isolines. These major simplifications afford, for the first time, analytical line shape formulas of arbitrarily polarized triplets as sums of elliptical integrals. Even with approximations applied, the analytical results agree almost perfectly with both simulated and experimental spectra and accurately capture the higher-order spectral effects such as peak shifts and net spin polarization. This universal scheme is also promising for other spectroscopic techniques in which anisotropy plays a significant role.

Introduction

Elucidation of the structures of materials and biological systems has been the everlasting topic for a wide variety of spectroscopies. Most of these techniques, except crystallography, reveal primarily a sample's scalar properties, such as the isotropic part of chemical shifts, dipole moments, spin couplings, and so on, which provide key information for the characterization and identification of a functional group, a molecule, or even a protein unit. As the research focuses have shifted from small compounds within isotropic solutions to bioactive macromolecules embedded in novel environments, there has been an increasing demand for the spatial parameters of the complex systems, that is, distances and orientations, for thorough understanding of their structure−function relationships and catalytic activities. In this regard, anisotropic sensitivity will be a powerful booster to the existing spectroscopic tools.

On the other hand, convolution of both the chemical and the orientational aspects of the analyte into the same spectrum leads to broadening, shifting, and/or overlapping of the spectral peaks. Moreover, because anisotropy is a three-dimensional property and most spectra are plotted against one independent variable, the reduction in dimensionality is made possible only by compressing the signals from many individual orientations into a single spectral point. Consequently, anisotropy was once considered an obstacle to better resolution and interpretation of a spectrum, rather than a depository of rich structural information. If these had not been a problem, then the anisotropy-eliminating experimental techniques, including solution-phase detection and magic-angle configurations, would not have been necessary.

As early as 1948, the two-dimensional anisotropy in the dipole−dipole interaction in two-proton systems was described,[1] well-known as the Pake doublet, which laid the foundation for solid-state nuclear magnetic resonance (SSNMR). Still, the experimental and theoretical handling of chemical-shift anisotropy and quadrupolar nuclei is currently a very active area.[2] Another popular tool for probing protein structure is fluorescence resonance energy transfer (FRET),[3] whose rate critically depends on the distance r and orientation factor κ^2 between the donor and acceptor chromophores. Unless κ^2 can be calculated or modeled with precision, the validity of the derived distances is questionable. A third example, electron paramagnetic resonance (EPR), is arguably one of the most anisotropic spectroscopies intrinsically, because the electron spin dipole is not only compact but also mobile, readily interacting with other types of angular momenta. The EPR powder pattern, essentially the three-dimensional version of the Pake doublet, was solved by Kneubühl in 1960.[4] Since then, the analysis of anisotropic EPR spectra has relied heavily upon computer simulations,[5−8] which outpaced the advances in theoretical approaches. In the following, we present a new and general methodology of tackling anisotropies in three dimensions in the context of EPR spectroscopy and believe that it can prove its effectiveness within a broader background.

Theroetical Basis

Anisotropy in Three Dimensions: The Ternary Diagram. In addition to the conventional Cartesian coordinates $\{x, y, z\}$ and spherical coordinates $\{r, \theta, \varphi\}$, the orientation of a vector V (e.g., spin angular momentum or magnetic field) of a three-dimensional space can be specified by a set of squares:

$$u = x^2/r^2 = \sin^2\theta\cos^2\varphi, v = y^2/r^2 = \sin^2\theta\sin^2\varphi, \quad w = z^2/r^2 = \cos^2\theta \qquad (1)$$

with the Pythagorean identity $u + v + w = 1$. Here, the new coordinates $\{u, v, w\}$ are unique only over the first octant, and only two of them are independent variables, although all three have equal physical significance. Cyclic variable substitutions such as relabeling $\{u, v, w\}$ with $\{v, w, u\}$ do not alter the

* Corresponding author. E-mail: m-wasielewski@northwestern.edu.

10.1021/jp103678m
Published on Web 07/27/2010

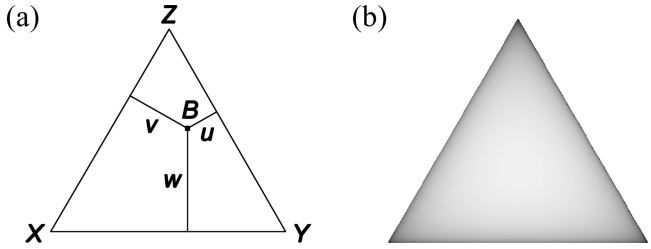

Figure 1. (a) The ternary diagram that represents squared Cartesian coordinates $\{u, v, w\}$. (b) A density plot in logarithm scale of the geometric weight $(uvw)^{-(1)/(2)}$ in eq 2, which approaches infinity at the dark vertices and sides where at least one of u, v, w vanishes.

nature of the problem. Accordingly, the Jacobian determinant for the change of variables is two-dimensional:

$$|J(u, v)| = |J(v, w)| = |J(w, u)| = \frac{1}{4 \sin \theta \sqrt{uvw}}$$

and the solid angle element of the new squared Cartesian coordinates is derived as

$$\mathrm{d}\Omega = |J(u, v)| \sin \theta \, \mathrm{d}\theta \, \mathrm{d}\varphi = \frac{\mathrm{d}v \, \mathrm{d}u}{4\sqrt{uvw}} \tag{2}$$

such that the definite integral

$$\int\int_{u+v+w=1} \mathrm{d}\Omega = \int_0^1 \int_0^{1-u} \frac{\mathrm{d}v \, \mathrm{d}u}{4\sqrt{uv(1-u-v)}} = \frac{\pi}{2}$$

gives one-eighth the surface area of a unit sphere. Equation 2 is a common geometric weight to apply to all three-dimensional anisotropies.

The energetic contribution to the anisotropic spectrum depends on the actual form of the Hamiltonian. For example, the effective scalar value of the electron **g** tensor can be expressed as the weighted root-mean-square of its three principal values, $g^2 = ug_{XX}^2 + vg_{YY}^2 + wg_{ZZ}^2$.[9] As for the spin dipole−dipole interaction[10]

$$H_{\mathrm{dipolar}} = S \cdot \mathbf{D} \cdot S = D_{XX} S_X^2 + D_{YY} S_Y^2 + D_{ZZ} S_Z^2 \tag{3}$$

S_k are the spin components, and **D** is the zero field splitting (zfs) tensor with its principal values D_{kk} ($k = X, Y, Z$). In the classical picture, we have the vector projection $S_k^2 = S^2 \cos^2 \angle Sk$, and $H_{\mathrm{dipolar}} = S^2(uD_{XX} + vD_{YY} + wD_{ZZ})$ is the scalar version of eq 3. The facts that g^2 and H_{dipolar} become linear expressions and that u, v, and w are normalized suggest that, although the anisotropic **D** and **g** tensors are usually visualized with three-dimensional spherical or ellipsoidal surfaces, planar ternary diagrams provide very useful additional insight into their physical nature, Figure 1. More importantly, the set of symmetric and linear coordinates drastically simplifies the mathematics, making analytical results achievable.

Results and Discussion

Molecular versus Laboratory Frames: First-Order Solutions. To start with, the spin Hamiltonian of a triplet state in an external field consists of a Zeeman term and a dipolar term

$$H = H_{\mathrm{Zeeman}} + H_{\mathrm{dipolar}} = g_{\mathrm{T}} \beta B \cdot S + S \cdot \mathbf{D} \cdot S \tag{4}$$

where g_{T} is the isotropic g factor of the triplet state, β is the Bohr magneton, and B is the external field. Even in this simple case, the two terms are not only noncommuting, but also within two different coordinate systems. The laboratory frame is defined by the orientation of B, whereas the principal axes of the zfs tensor **D** establish the molecular frame $\{X, Y, Z\}$. Unless in crystalline phases, there are no restrictions on the relationship between these two frames. In this Article, we fix the molecular frame and consider the external field B being applied along all possible directions in the first octant, Figure 1.

Because of the noncollinearity of the two coordinate systems, eq 4 does not have closed exact solutions except when B is along the canonical orientation X, Y, or Z. Instead, computer line shape simulations employ numerical diagonalization at discrete field orientations. Nevertheless, in typical EPR experiments of triplet states, the external field B is always dominating ($D/B \approx 10^{-1}$), and the dipolar term can be treated as a perturbation. This assumption is equivalent to assuming that the spin angular momentum remains quantized along B, even in the presence of the dipole−dipole interaction. The first-order energy levels of eq 4 are then obtained as[5]

$$\begin{aligned} E_0^{(1)} &= -\left(w - \frac{1}{3}\right)D - (u - v)E \\ E_{\pm 1}^{(1)} &= \pm g_{\mathrm{T}} \beta B - \frac{1}{2} E_0^{(1)} \end{aligned} \tag{5}$$

where $D = 3/2D_{ZZ}$, $E = 1/2(D_{XX} - D_{YY})$ are the zfs parameters, and u, v, w are the Cartesian squares as mentioned earlier. Once again, these first-order energies appear as linear functions of u, v, and w, and so do the $\Delta m_{\mathrm{S}} = 1$ transition energies:

$$\Delta E_{0\to 1}^{(1)}(u, v, w) = g_{\mathrm{T}} \beta B - \frac{1}{2} D + \frac{3}{2}[(u - v)E + wD] \tag{6a}$$

$$\Delta E_{-1\to 0}^{(1)}(u, v, w) = g_{\mathrm{T}} \beta B + \frac{1}{2} D - \frac{3}{2}[(u - v)E + wD] \tag{6b}$$

Because eqs 7a and b differ only by the signs of D and E, we shall focus on the 0→1 transition first, and then apply the results to the −1→0 transition by simply switching the signs of D and E.

Field-Swept EPR Spectra. Continuous-wave (c.w.) EPR spectra are acquired by fixing the microwave excitation frequency ν while changing the external field B. Hereupon, the microwave energy is more conveniently expressed in magnetic units by $B_0 = h\nu/g_{\mathrm{T}}\beta$, and the D and E parameters are likewise converted into magnetic units. All paramagnetic centers in accord with the resonance condition

$$\Delta E^{(1)} = g_{\mathrm{T}} \beta B_0 \tag{7}$$

contribute to the spectral intensity I in arbitrary units by $I_{\mathrm{i}\to\mathrm{f}} = \sum_{\mathrm{resonant}} T_{\mathrm{i}\to\mathrm{f}} P_{\mathrm{if}}$, where i and f stands for initial and final sublevels, respectively, $T_{\mathrm{i}\to\mathrm{f}}$ for transition probability, and $P_{\mathrm{if}} = \rho_{\mathrm{i}} - \rho_{\mathrm{f}}$ for spin polarization. The sum runs over all resonant transitions. Because the probability for allowed single-quantum EPR transitions is unity to all orders of perturbation, the T factor is

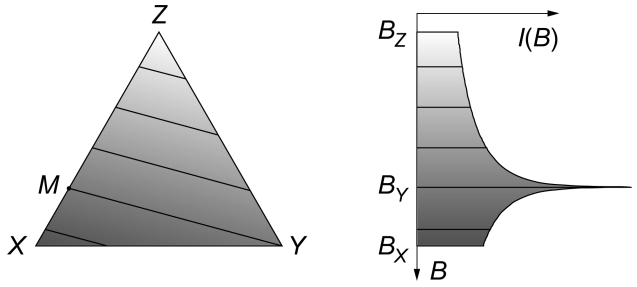

Figure 2. The isolines for the 0→1 transition on the ternary plot (left), each contributing to one spectral point $I(B)$ (right). Darker areas correspond to higher resonance magnetic fields.

hereupon dropped. In the squared Cartesian coordinates, the above summation turns into a path integral:

$$I_{0\rightarrow 1}(B) = \int_{\text{eq 7, } u+v+w=1, u,v,w\geq 0} \frac{P_{01}\,\mathrm{d}v}{4\sqrt{uvw}} \tag{8}$$

and similarly for the −1→0 transition. Here, the solid angle element dΩ has already been included.

Considering the extremes first, we let B_X, B_Y, and B_Z denote the three principal values of the resonant field. Again, they show up on an EPR spectrum as the turning points, Figure 2. Manipulation of eq 6 gives

$$B_X = B_0 \pm \frac{1}{2}(D - 3E), B_Y = B_0 \pm \frac{1}{2}(D + 3E), B_Z = B_0 \mp D, \begin{cases} + \text{ for } 0 \rightarrow 1 \\ - \text{ for } -1 \rightarrow 0 \end{cases} \tag{9}$$

where B_0 is positioned at the center of spectrum. As for the intermediate orientations, the resonance field and the squared Cartesian coordinates are linearly interconvertible:

$$B_{\text{res}} = uB_X + vB_Y + wB_Z \tag{10}$$

$$u = (\Delta_{BZ} - v\Delta_{YZ})/\Delta_{XZ}, w = (\Delta_{XB} - v\Delta_{XY})/\Delta_{XZ} \tag{11}$$

Here, the Δ_{jk}'s are shorthands for the differences $\Delta_{YZ} = B_Y - B_Z$, $\Delta_{XB} = B_X - B_{\text{res}}$, etc. The integration limit in eq 8 can be determined along with the condition $0 \leq u, v, w \leq 1$.

Isolines in the Squared Cartesian Coordinates. A more visual approach is to view eq 11 as a family of parallel lines in the squared Cartesian coordinates, each corresponding to a resonance field value, Figure 2. It is noteworthy that only one of these isolines can cross a vertex of the ternary plot under any circumstance. For typical triplet states, $D > -3E \geq 0$,[5,10] or in other words $B_Z < B_Y \leq B_X$ for the 0→1 transition and $B_Z > B_Y \geq B_X$ for the −1→0 transition. Therefore, the vertex to be crossed is Y, and the intersection on the XZ side is denoted $M(u_0, 0, w_0)$: $u_0 = \Delta_{YZ}/\Delta_{XZ}$, $w_0 = \Delta_{XY}/\Delta_{XZ}$, which means that all of the points on the isoline MY contribute to the spectral intensity $I(B_Y)$. For the same reason, the area between B_X and B_Y of an EPR spectrum originates from triangle MXY on the diagram and the rest from triangle MYZ, Figure 2.

In eq 8, the solid angle element dΩ approaches infinity at the vertices X, Y, or Z. Hence $I(B_Y)$, a line integral that crosses Y, is the one and only singularity on the EPR spectrum. For the other field values, eq 8 becomes

$$I_{0\rightarrow 1}(B) = \frac{\Delta_{XZ}}{4}\int_0^{v_{\max}} \frac{P_{01}\,\mathrm{d}v}{\sqrt{(\Delta_{BZ} - v\Delta_{YZ})v(\Delta_{XB} - v\Delta_{XY})}} \tag{12}$$

with the upper integral limit $v_{\max} = \Delta_{BZ}/\Delta_{YZ}$ for $B_Z \leq B < B_Y$ and $v_{\max} = \Delta_{XB}/\Delta_{XY}$ for $B_Y \leq B < B_X$. Here again, the Δ's stand for field differences. The spin polarization term P_{01} is determined by the specific mechanism that populates the triplet sublevels.

Isotropic Sublevel Populations: Radical Pair Mechanism versus Boltzmann Distribution. In the radical-pair intersystem crossing mechanism (RP-ISC),[11−13] the triplet sublevel T_0 is mixed with the original singlet state, S, due to their energetic proximity. Consequently, T_0 accommodates all of the population from ISC, and the other two sublevels $T_{\pm 1}$ are vacant, regardless of the spatial orientation of the molecule: $\rho_0 = 1$, $\rho_{\pm 1} = 0$, $P_{01} = \rho_0 - \rho_1 = 1$, and $P_{-10} = \rho_{-1} - \rho_0 = -1$. In this case, eq 12 is evaluated to be

$$I_{0\rightarrow 1}(B) = \begin{cases} \dfrac{K(Q)}{2\sqrt{\Delta_{XB}\Delta_{YZ}}} & \text{for } B_Z \leq B < B_Y \\ \dfrac{K(Q^{-1})}{2\sqrt{\Delta_{XY}\Delta_{BZ}}} & \text{for } B_Y < B \leq B_X \end{cases} \tag{13}$$

where $Q = ((\Delta_{XY}\Delta_{BZ})/(\Delta_{XB}\Delta_{YZ}))^{1/2}$ and $K(k) = \int_0^1 (\mathrm{d}t)/((1 - t^2)^{1/2}(1 - k^2t^2)^{1/2})$ is the complete elliptic integral of the first kind. Line shape expressions of a similar form have been reported[4,9] for transition metal ions with anisotropic **g** tensors, also known as the "powder pattern". The full triplet spectrum is simply the sum of two transitions, resulting in two sets of distinct turning points along the X, Y, and Z orientations, Figure 3.

To the first-order approximation, the Boltzmann distribution among the triplet sublevels is

$$\rho_i \approx \exp\left(-\frac{ig_{\text{T}}\beta B}{k_{\text{B}}T}\right) \approx 1 - \frac{ig_{\text{T}}\beta B}{k_{\text{B}}T}, i = -1, 0, 1,$$

and the thermal polarization is thus a positive constant $P_{01} = P_{-10} = g_{\text{T}}\beta B/k_{\text{B}}T$. Here, $k_{\text{B}}T$ is the thermal energy, and B is assumed to vary only within a small range. If not, thermal polarization needs to be considered anisotropic, and the treatment becomes more complicated.

Anisotropic Sublevel Populations: Spin−Orbit Intersystem Crossing. When intersystem crossing occurs under the influence of spin−orbit interaction, molecular orbital symmetries serve as a crucial factor. A parametric model is that SO interaction induces triplet states with their spin angular momentum quantized along the molecular axes X, Y, and Z, with population fractions A_X, A_Y, and A_Z, respectively.[14] In the presence of a dominating external field, the sublevel populations need to be transformed from the zero-field basis $T_{X,Y,Z}$ to the high-field basis $T_{-1,0,1}$. The first-order result reads

$$\rho_0 = uA_X + vA_Y + wA_Z, \rho_{\pm 1} = \frac{1}{2}(1 - \rho_0)$$

or in terms of spin polarization: $P_{01} = -P_{-10} = 1/2[3(uA_X + vA_Y + wA_Z) - 1]$. An intuitive way is to express P_{01} and P_{-10} in terms of their X, Y, and Z components:

$$P_{01} = -P_{-10} = uP_X + vP_Y + wP_Z, P_k = \frac{1}{2}(3A_k - 1), \quad k = X, Y, Z \tag{14}$$

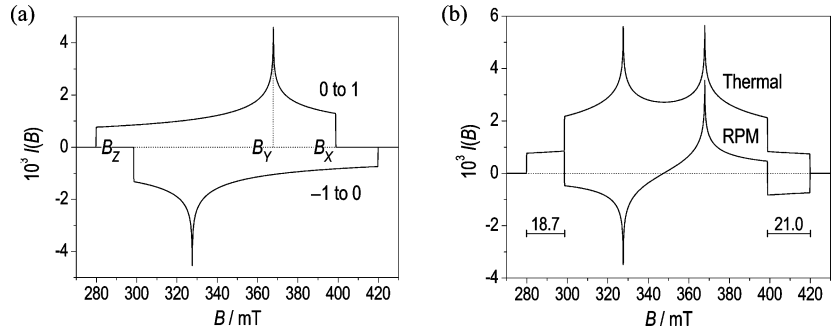

Figure 3. EPR triplet line shapes according to eq 13 with $B_0 = 350$ mT, $D = 70$ mT, and $E = -10$ mT. (a) The individual $\Delta m_S = 1$ transitions, one in absorption and the other in emission. (b) The full EPR spectra of triplets from the radical pair mechanism (see text) or thermal equilibrium with the same parameters. The high-field "shoulder" is a little wider than the low-field one due to higher-order corrections.

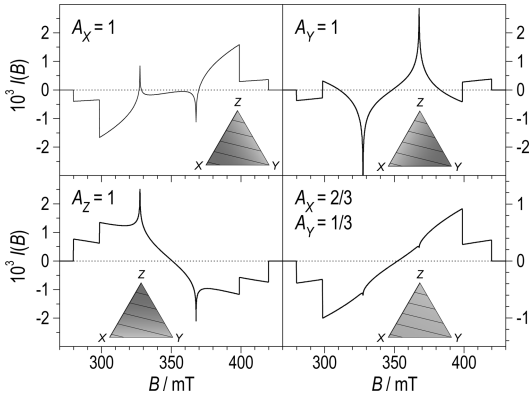

Figure 4. Typical EPR triplet line shapes with anisotropic spin polarizations due to spin−orbit interaction with the parameters $A_{X,Y,Z}$ listed and B_0, D, E the same as in Figure 3. In each panel, the color-coded ternary diagram with field isolines illustrates the anisotropic spin polarization within the 0→1 transition, with red indicating an absorptive polarization ("a"), blue an emissive one ("e"), and gray none.

Inserting eqs 11 and 14 into eq 12 and integration afford

$$I_{0\to1}(B) = \begin{cases} \dfrac{(\Delta_{XB}P_Y - \Delta_{YB}P_X)\,K(Q) + C\Delta_{XB}\,E(Q)}{2\Delta_{XY}\sqrt{\Delta_{XB}\Delta_{YZ}}} & \text{for } B_Z \le B < B_Y \\ \dfrac{(\Delta_{BZ}P_Y - \Delta_{BY}P_Z)\,K(Q^{-1}) + C\Delta_{BZ}\,E(Q^{-1})}{2\Delta_{YZ}\sqrt{\Delta_{XY}\Delta_{BZ}}} & \text{for } B_Y < B \le B_X \end{cases} \quad (15)$$

where Q and $K(k)$ are defined as above, $C = (\Delta_{YZ}P_X + \Delta_{ZX}P_Y + \Delta_{XY}P_Z)/\Delta_{XZ}$ is a constant, and $E(k) = \int_0^1((1 - k^2t^2)/(1 - t^2))^{1/2}\,dt$ is the complete elliptic integral of the second kind. Several examples of eq 15 are plotted in Figure 4.

Higher-Order Corrections to Energy Levels and Populations. In the above, we have been able to evaluate the spectral intensity in eq 8 and arrive at analytical line shape formulas for triplets caused by the radical pair and SO intersystem crossing mechanisms. These unprecedented results are made possible because the two key factors, resonance field B and spin polarization P, both turn out to be linear functions of the squared Cartesian coordinates u, v, and w:

$$B_{res} = uB_X + vB_Y + wB_Z \quad (10a)$$

$$P_{01} = -P_{-10} = uP_X + vP_Y + wP_Z \quad (14a)$$

However, these are derived on the basis of the first-order approximation; exact solutions to the Hamiltonian (eq 4) are mathematically intractable except at the canonical orientations X, Y, and Z. As a rational compromise, B_k and P_k ($k = X, Y, Z$) can be calculated exactly and applied into the first-order linear relationships, eqs 10 and 14, which then enhances the accuracies of all of the intermediate orientations. It is noteworthy that the first-order formulas, eqs 13 and 15, remain unchanged; they produce more accurate triplet line shapes by taking improved parameters.

Listed below are the exact values of B_k and P_k:[15]

$$B_X = B_X^{(1)} + \frac{1}{2}(D + E)\tan\theta_X, B_Y = B_Y^{(1)} - \frac{1}{2}(D - E)\tan\theta_Y, B_Z = B_Z^{(1)} - E\tan\theta_Z \quad (16)$$

$$P_k = P_k^{(1)} + \frac{1}{2}(A_{k+1} - A_{k+2})\sin 2\theta_k, k = X,Y,Z \quad (17)$$

In the above formulas, θ_k values describe the degree of deviation from the high-field limit:

$$\tan 2\theta_X = -\frac{D + E}{2B_X}, \tan 2\theta_Y = \frac{D - E}{2B_Y}, \tan 2\theta_Z = \frac{E}{B_Z}, -\frac{\pi}{4} < \theta_k < \frac{\pi}{4} \quad (18)$$

It makes good sense that the field values appear in the denominators. Yet, an issue arises that in field-swept EPR, B can take on a wide range of values. Therefore, to obtain the exact solutions, eqs 16 and 18 need to be combined and solved by iteration. In practical calculations, the first-order values $B_k^{(1)}$ are accurate enough to be used directly in eq 18. As for EPR spectra acquired in the frequency space, the fixed external field value shall be employed.

Higher-Order Effects on Triplet EPR Spectra and Spin Polarizations. The first-order triplet spectrum, with both the 0→1 and the −1→0 transitions, is central symmetric. The center field B_0 reflects the microwave quantum in magnetic units. When the dipolar interaction (eq 3) is taken into account, it provides a double-quantum coupling between the T_1 and T_{-1} states, bringing the former higher in energy and the latter lower. As a

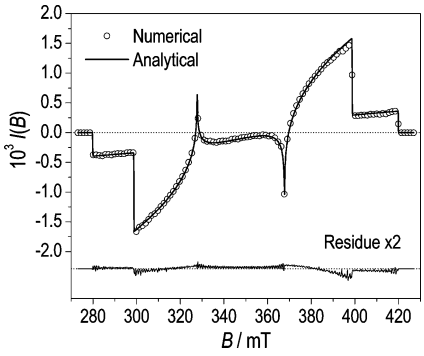

Figure 5. Comparison between the line shapes calculated for $A_X = 1$, using eq 15 (solid line) and numerical simulation (○). Their difference is magnified on the bottom.

result, the single quantum transitions require less Zeeman splitting to match that microwave energy. Quantitatively, it can be shown that all of the correction terms in eq 16 are negative, regardless of the signs of D and E. This leads to a down shift of an actual spectrum as compared to its first-order approximation, with the X edge affected most and the Z edge least, assuming $D > -3E \geq 0$ (see Figure 3).

To accurately estimate spin polarization, which is a first-order quantity, higher-order effects need to be taken into account. For instance, the "magic orientation" as defined by $u = v = w = 1/3$ is the orientation most removed from all three canonical ones, X, Y, and Z, where exact solutions are available in eq 17. A linear extrapolation at the magic orientation according to eq 14 gives

$$P_{-10}^{(1)} = P_{01}^{(1)} \approx \frac{1}{12}\left[(3A_Z - 1)\frac{D}{B_0} + 3(A_X - A_Y)\frac{E}{B_0}\right]$$

whereas a direct solution outlined in the Appendix affords

$$P_{-10} = P_{01} \approx \frac{1}{6}\left[(3A_Z - 1)\frac{D}{B_0} + 3(A_X - A_Y)\frac{E}{B_0}\right] \tag{19}$$

Note that the linear prediction, extended farthest in this case, is off by one-half the actual result. To remedy this deviation, it is desirable to make the magic orientation a new reference point in addition to the canonical orientations and interpolate toward the regions in between:

$$P_X^{(2)} = P_X^{(1)} + \frac{5 - 3u}{4}(A_Y - A_Z) \times \tan 2\theta_X, \text{likewise for } P_Y^{(2)} \text{ and } P_Z^{(2)}$$

Combined with eq 14, an integral over all of the spatial orientations yields the net spin polarization for each transition:

$$P_{01}^{\text{net}} = P_{-10}^{\text{net}} = \frac{2}{15}\left[(3A_Z - 1)\frac{D}{B_0} + 3(A_X - A_Y)\frac{E}{B_0}\right] \tag{20}$$

which agrees with the result of earlier derivations.[16,17] By summing these two transitions, the net spin polarization gets doubled up. In the case of axial symmetry with Z dominance ($A_X = A_Y < 1/3 < A_Z$), such as zinc tetraphenylporphyrin (ZnTPP), absorptive spin polarization is generated in the triplet sublevels, Figure 6b. In contrast, the free-base tetraphenylporphyrin (TPP) lacks a d_{z^2} orbital, and its SO-induced triplet state is overall emissive. It should be emphasized that even in isotropic solutions where molecules tumble fast and each of them samples all possible orientations, most of the EPR spectral features get averaged out, but the net spin polarization remains a single peak.[18] This model constitutes the triplet mechanism in the theory of chemically induced dynamic electron polarization (CIDEP).[19]

Comparison between Analytical, Numerical, and Experimental Results. The numerical simulation of a triplet EPR line shape is comprised of the following: (1) discretize the spatial orientations of the external field B; (2) numerically diagonalize the spin Hamiltonian (eq 4) at each orientation to yield energy levels and populations; and (3) plot the simulation result as a histogram of spectral intensity versus field value bins. Figure 5 shows the line shape of a SO-induced triplet with $A_X = 1$, calculated both numerically and analytically. It is beyond our expectation that these two curves agree so well, suggesting that although the analytical formulas, eqs 13 and 15, are not exact solutions, they are accurate enough even without the time-consuming matrix diagonalizations and nested loops. The discrepancy between the two outputs can be attributed to sources such as the discretization error in the numerical method and the linear approximation (eqs 10 and 14) underlying the analytical formulas.

Experimentally, spin-polarized triplet states are generated in a variety of photochemical systems ranging from small organic molecules to the green-plant photosynthetic reaction center. Shown in Figure 6a is the EPR spectrum of an artificial photosynthesis compound[20,21] measured in frozen toluene at 100 K, which undergoes radical-pair intersystem crossing and exhibits the characteristic line shape predicted by eq 13. The narrow signal in the middle of the spectrum represents the radical pair intermediate. Figure 6b depicts the photoinduced triplet state of zinc tetraphenylporphyrin, ^{3*}ZnTPP, in a 2-methyltetrahydrofuran (MTHF) glass at 10 K.[22] In this planar molecule, the central zinc atom intensifies the spin−orbit interaction along the Z axis, and accordingly the experimental spectrum matches eq 15 excellently with $A_Z = 1$ and $A_X = A_Y = 0$. Additionally, the theoretical results replicate the higher-order features nicely in both situations. In Figure 6a, the spectral "shoulder" on the right is slightly wider than the one on the left. Also, in Figure 6b, the upward bending of the spectrum, that is, the net absorptive spin polarization, is evident.

Anisotropic Orientation: Triplets in Nematic Liquid Crystals. Liquid crystals (LCs) in the nematic phase exhibit long-range orientational order L and rod-like molecules embedded in them are oriented parallel. Depending on the anisotropic magnetic susceptibility of a nematic LC, it can be aligned either parallel or perpendicular to a strong enough magnetic field B.

In the ideal situation where all molecules have identical orientations relative to the external field, anisotropy no longer exists or is reduced to two dimensions, of which solutions have been known. In practice, the molecular orientation fluctuates around an expectation value defined by the direction of B. Consider a simple case in which the molecular backbone is aligned in a nematic LC so that, on average, the triplet Y axis is parallel to B. A normal distribution has been used to describe the fluctuation in $\angle BY$: $f_{\parallel}(\angle BY) = \exp(-\angle BY^2/2\sigma^2)$,[20] which, however, is difficult to include in an elliptical integral such as

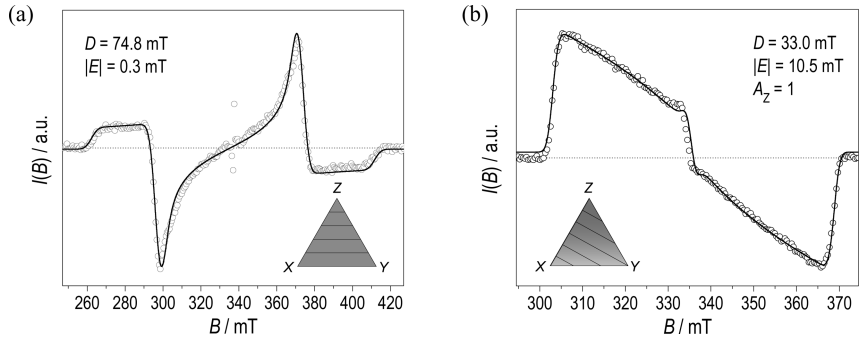

Figure 6. Comparison between the theoretical (solid line) and experimental (○) line shapes of triplet states induced by (a) the radical pair mechanism and (b) the spin−orbit mechanism. The ternary plots (insets) have the same meaning as in Figure 4.

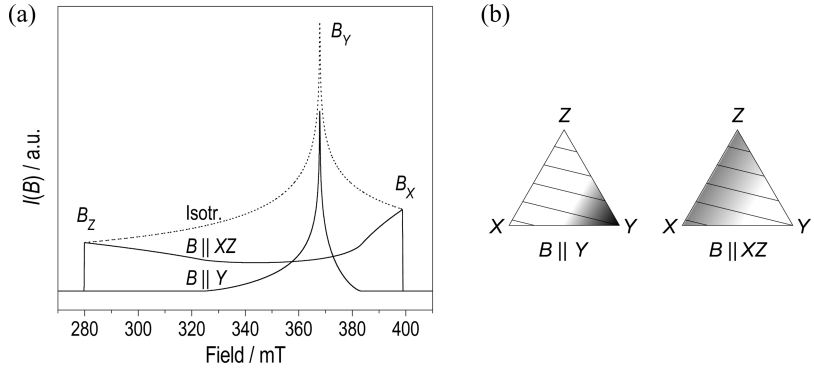

Figure 7. (a) Unnormalized EPR line shapes of triplets partially aligned in a nematic liquid crystal, with the magnetic field parallel ($B||Y$) and perpendicular ($B||XZ$) to the Y triplet direction. In both cases, only one transition is plotted, and the alignment parameter $R = 2$ (see text). A line shape for isotropic media (dotted line) is also included for comparison. (b) The ternary diagrams with isolines show the distribution profiles of the field orientations with respect to the triplet axes, with darkness proportional to the probability.

eq 12. Alternatively, a Boltzmann-type model of angular distribution is, again, based on a Cartesian square:

$$f_{\parallel}(\angle BY) = 1 - \frac{E_{\perp} - E_{\parallel}}{k_{\mathrm{B}}T}\sin^2\angle BY = 1 - R(1 - v), v = \cos^2\angle BY = y^2/r^2 \quad (21)$$

It can be shown that upon $R = (2\sigma^2)^{-1}$ these two models display the same behavior to the first order, whereas eq 21, a linear function of v, facilitates mathematical manipulations significantly. By requiring $f_{\parallel}(\angle BY) \geq 0$, we get $\cos^2\angle BY \geq 1 - R^{-1}$, implying that $\angle BY$ can fluctuate only within a limited range, which is a reasonable assumption.

Incorporation of the distribution function eq 21 into the integral in eq 12 leads to a sum of incomplete elliptic integrals:

$$I_{0\rightarrow 1}(B) = \begin{cases} \frac{1}{\sqrt{\Delta_{XB}\Delta_{YZ}}}[F(\lambda;Q) - R\frac{\Delta_{BY}}{\Delta_{XY}}(F(\lambda;Q) - \frac{\Delta_{XZ}}{\Delta_{YZ}}\Pi(\lambda;Q^2,Q))] & \text{for } B_Z \leq B < B_Y \\ \frac{1}{\sqrt{\Delta_{XY}\Delta_{BZ}}}[F(\lambda^{-1};Q^{-1}) - R\frac{\Delta_{YB}}{\Delta_{YZ}}(F(\lambda^{-1};Q^{-1}) - \frac{\Delta_{XZ}}{\Delta_{XY}}\Pi(\lambda^{-1};Q^{-2},Q^{-1}))] & \text{for } B_Y < B \leq B_X \end{cases} \quad (22)$$

where $\lambda = ((\Delta_{XB}(\Delta_{YZ} + R\Delta_{BY}))/(\Delta_{BZ}(\Delta_{XY} - R\Delta_{BY})))^{1/2}$, $F(x; k) = \int_0^x(\mathrm{d}t)/((1 - t^2)^{1/2}(1 - k^2t^2)^{1/2})$ is the incomplete elliptic integral of the first kind, and $\Pi(x; n, k) = \int_0^x(1)/(1 - nt^2)(\mathrm{d}t)/((1 - t^2)^{1/2}(1 - k^2t^2)^{1/2})$ is the incomplete elliptic integral of the third kind.[23] Because by assumption $\angle BY$ is just allowed to sample a confined set of values, spectra calculated according to eq 22 do not cover the full extent as in isotropic media, Figure 7.

In a second case, the nematic LC is aligned perpendicular to the external field. Next, the distribution function eq 21 becomes $f_{\perp}(\angle BY) = 1 - Rv$ with $R = (E_{\parallel} - E_{\perp})/k_{\mathrm{B}}T$, indicating that $\angle BY$ takes on values only in the proximity of $\pi/2$. Similarly, evaluation of the integral in eq 12 gives

$$I_{0\rightarrow 1}(B) = \begin{cases} \frac{1}{\sqrt{\Delta_{XB}\Delta_{YZ}}}[(1 - R)\bar{F}(\lambda;Q) + R\frac{\Delta_{BY}}{\Delta_{XY}}(\bar{F}(\lambda;Q) - \frac{\Delta_{XZ}}{\Delta_{YZ}}\bar{\Pi}(\lambda;Q^2,Q))] & \text{for } B_Z \leq B < B_Y \\ \frac{1}{\sqrt{\Delta_{XY}\Delta_{BZ}}}[(1 - R)\bar{F}(\lambda^{-1};Q^{-1}) + R\frac{\Delta_{YB}}{\Delta_{YZ}}(\bar{F}(\lambda^{-1};Q^{-1}) - \frac{\Delta_{XZ}}{\Delta_{XY}}\bar{\Pi}(\lambda^{-1};Q^{-2},Q^{-1}))] & \text{for } B_Y < B \leq B_X \end{cases} \quad (23)$$

where $\lambda = ((\Delta_{XB}(\Delta_{YZ} - R\Delta_{BZ}))/(\Delta_{BZ}(\Delta_{XY} - R\Delta_{XB})))^{1/2}$ and the overscored functions are the differences of complete and incomplete elliptical integrals of the same kind: $\bar{F}(x; k) = F(1; k) - F(x; k)$ and $\bar{\Pi}(x; k) = \Pi(1; k) - \Pi(x; k)$. In Figure 7, the plot of eq 23 resembles the two-dimensional (XZ plane) anisotropy situations in that the X and Z edges become sharper and the Y singularity is absent, while the ratio of spectral intensities at the X and Z edges is maintained, as compared to the isotropic case.

Besides the Y axis, the X and Z axes of the molecular frame can be aligned either parallel or perpendicular to the external field. The above treatment also works for these cases, and the results bear the same shape as eqs 22 and 23, albeit more complicated. In general, as long as the distribution function has a linear form, the integral in eq 12 is manageable and can be evaluated analytically as a sum of elliptical integrals.

Conclusions

In three-dimensional spaces, the Cartesian and spherical coordinates are the two systems most widely applied. They are especially convenient for objects with cuboidal and axial symmetry, respectively. One shortcoming of the spherical coordinates is that the azimuthal angle φ (the colatitude) and the polar angle θ (the longitude) are not interchangeable, rendering complications in the mathematics. In a system with one anisotropic term (e.g., zfs tensor $\mathbf{D}$) or more than one collinear anisotropic term (e.g., zfs plus SO-ISC), both axial and rhombic symmetries are possible, and the three principal axes X, Y, and Z are cyclically symmetric. A combination of the benefits of these two coordinate systems prompted the construction of the squared Cartesian coordinates and its corresponding ternary diagram, which linearize and symmetrize the expressions of all anisotropic variables covered in this work, and thus lead to the analytical formulas for EPR line shapes of arbitrarily polarized triplet states.

It is beneficial to compare the two anisotropies, closely related and common in solid-state magnetic resonance: those of chemical shift ($\mathbf{g}$ or σ) and spin dipole−dipole interaction ($\mathbf{D}$). Their Hamiltonians, $\beta B\cdot\mathbf{g}\cdot S$ and $S\cdot\mathbf{D}\cdot S$, take essentially the same mathematical form. Yet, the nuance between the field B and spin S, a classical vector and a quantized one, makes the distinction in the treatment of their physics. This is because the magnetic field can be projected onto the three principal axes of the molecular frame, $B_k = B\cos\angle Bk$ ($k = X, Y, Z$), which is indispensable to calculating the exact line shape for an anisotropic $\mathbf{g}$ tensor.[4,9] On the other hand, this projection relationship cannot be directly translated into a quantum version in terms of the spin S, because $S_X^2 + S_Y^2 + S_Z^2 = S^2 = S(S+1)$. This is to say that treating a quadratic term like $S\cdot\mathbf{D}\cdot S$ classically implies an approximation. In NMR, the dipolar interaction is much weaker than the Zeeman term by a factor of $\sim 10^{-5}$, and thus first-order perturbation suffices for the derivation of the Pake doublet formula. However, in X-band EPR, due to the compactness and mobility of electron spin dipoles, the ratio D/B_0 is typically 10^{-1}. To carry out higher-order corrections, our method is to incorporate high-order parameters (energies and spin polarizations) into the first-order line shape formulas, which has proved convenient and very successful.

To the best of our knowledge, the various triplet EPR line shape formulas presented in this work, eqs 13, 15, 22, and 23, have not been reported before. These analytical formulas make the analysis of experimental spectra substantially faster, as compared to fully numerical simulation routines, with virtually no loss in accuracy. More importantly, instead of accepting the simulated results simply as is, we are now enabled to understand and predict many properties of a three-dimensional anisotropic system, and we are confident that this methodology will quickly find its way to addressing new applications such as EPR spectra with $S > 1$ and quadrupolar NMR spectra.

Acknowledgment. This work was supported by the National Science Foundation, under Grant No. CHE-0718928 (M.R.W.). M.A.R. thanks the NSF for partial support under the CHE and MRSEC divisions as well as ONR-Chemistry. Q.M. acknowledges Dr. Zachary E. X. Dance for his assistance in the EPR experiments and for helpful discussions. We are indebted to the anonymous reviewers for their careful reading and valuable criticisms.

Appendix: Mathematical Derivation of Eq 19

The term "magic orientation" refers to the orientation in which the external field B spans a magic angle from each of the molecular axes X, Y, and Z. In terms of the squared Cartesian coordinates, $u = v = w = 1/3$. The zfs interaction term reads

$$H_{\mathrm{zfs}} = D\left(S_Z^2 - \frac{2}{3}\right) + E(S_X^2 - S_Y^2) = \frac{D}{3}\begin{pmatrix} 0 & -1 & 1 \\ -1 & 0 & 1 \\ 1 & 1 & 0 \end{pmatrix} + \frac{\mathrm{i}E}{\sqrt{3}}\begin{pmatrix} 0 & -1 & -1 \\ 1 & 0 & 1 \\ 1 & -1 & 0 \end{pmatrix}\begin{matrix} |\mathrm{T}_{-1}\rangle \\ |\mathrm{T}_0\rangle \\ |\mathrm{T}_1\rangle \end{matrix}$$

whose eigenvectors constitute the transformation matrix from the high-field basis $\mathrm{T}_{-1,0,1}$ to the molecular basis $\mathrm{T}_{X,Y,Z}$:

$$\begin{matrix} |\mathrm{T}_X\rangle \\ |\mathrm{T}_Y\rangle \\ |\mathrm{T}_Z\rangle \end{matrix} = \frac{1}{\sqrt{3}}\begin{pmatrix} e^{-\mathrm{i}2\pi/3} & 1 & e^{-\mathrm{i}\pi/3} \\ e^{\mathrm{i}2\pi/3} & 1 & e^{\mathrm{i}\pi/3} \\ 1 & 1 & -1 \end{pmatrix}\begin{matrix} |\mathrm{T}_{-1}\rangle \\ |\mathrm{T}_0\rangle \\ |\mathrm{T}_1\rangle \end{matrix}$$

Provided that $D, E \ll B_0$, the first-order solution to the full Hamiltonian, eq 4, is evaluated to be

$$\begin{matrix} |\mathrm{T}'_{-1}\rangle \\ |\mathrm{T}'_0\rangle \\ |\mathrm{T}'_1\rangle \end{matrix} = \begin{pmatrix} 1 & (D - \mathrm{i}\sqrt{3}E)/3B_0 & -(D + \mathrm{i}\sqrt{3}E)/6B_0 \\ -(D - \mathrm{i}\sqrt{3}E)/3B_0 & 1 & -(D - \mathrm{i}\sqrt{3}E)/3B_0 \\ (D + \mathrm{i}\sqrt{3}E)/6B_0 & (D - \mathrm{i}\sqrt{3}E)/3B_0 & 1 \end{pmatrix}\begin{matrix} |\mathrm{T}_{-1}\rangle \\ |\mathrm{T}_0\rangle \\ |\mathrm{T}_1\rangle \end{matrix}$$

along with the sublevel populations from spin−orbit intersystem crossing:

$$\rho_0 = \sum_{k=X,Y,Z} A_k |\langle \mathrm{T}'_0|\mathrm{T}_k\rangle|^2 \approx \frac{1}{3} + \frac{2}{3}(A_X - A_Y)\frac{E}{B_0}$$

$$\rho_{\pm 1} = \sum_{k=X,Y,Z} A_k |\langle \mathrm{T}'_{\pm 1}|\mathrm{T}_k\rangle|^2 \approx \frac{1}{3} \mp \frac{3A_Z - 1}{6}\frac{D}{B_0} + \frac{A_X - A_Y}{2}\frac{E}{B_0}$$

Finally, the spin polarization turns out to be

$$P_{-10} = P_{01} = \frac{1}{6}\left[(3A_Z - 1)\frac{D}{B_0} + 3(A_X - A_Y)\frac{E}{B_0}\right] \tag{19a}$$

References and Notes

(1) Pake, G. E. *J. Chem. Phys.* **1948**, *16*, 327–336.
(2) Laws, D. D.; Bitter, H.-M. L.; Jerschow, A. *Angew. Chem., Int. Ed.* **2002**, *41*, 3096–3129.

(3) Lakowicz, J. R. *Principles of Fluorescence Spectroscopy*, 2nd ed.; Kluwer Academic/Plenum: New York, 1999.
(4) Kneubühl, F. K. *J. Chem. Phys.* **1960**, *33*, 1074–1078.
(5) Wasserman, E.; Yager, W. A.; Snyder, L. C. *J. Chem. Phys.* **1964**, *41*, 1763–1772.
(6) Stoll, S. D. Sc. thesis, Eidgenössische Technische Hochschule Zürich, 2003.
(7) Blank, A.; Levanon, H. *Concepts Magn. Reson., Part A* **2005**, *25*, 18–39.
(8) Stoll, S.; Schweiger, A. *J. Magn. Reson.* **2006**, *178*, 42–55.
(9) Beltrán-López, V.; Mile, B.; Rowlands, C. C. *J. Chem. Soc., Faraday Trans.* **1996**, *92*, 2303–2310.
(10) Carrington, A.; McLachlan, A. D. *Introduction to Magnetic Resonance with Applications to Chemistry and Chemical Physics*; Harper and Row: New York, 1967.
(11) Closs, G. L.; Forbes, M. D. E.; Norris, J. R. *J. Phys. Chem.* **1987**, *91*, 3592–3599.
(12) Hoff, A. J. *Advanced EPR: Applications in Biology and Biochemistry*; Elsevier: Amsterdam/New York, 1989; pp 405−440.
(13) Norris, J. R.; Morris, A. L.; Thurnauer, M. C.; Tang, J. *J. Chem. Phys.* **1990**, *92*, 4239–4249.
(14) Levanon, H.; Norris, J. R. *Chem. Rev.* **1978**, *78*, 185–198.
(15) Stevens, K. W. H. *Proc. R. Soc. London, Ser. A* **1952**, *214*, 237–246.
(16) Wong, S. K.; Hutchinson, D. A.; Wan, J. K. S. *J. Chem. Phys.* **1973**, *58*, 985–989.
(17) Atkins, P. W.; Evans, G. T. *Mol. Phys.* **1974**, *27*, 1633–1644.
(18) Yamauchi, S. *Bull. Chem. Soc. Jpn.* **2004**, *77*, 1255–1268.
(19) *Chemically Induced Magnetic Polarization*; Muus, L. T., Atkins, P. W., McLauchlan, K. A., Pedersen, J. B., Eds.; Reidel: Dordrecht/Boston, 1977.
(20) Hasharoni, K.; Levanon, H.; Greenfield, S. R.; Gosztola, D. J.; Svec, W. A.; Wasielewski, M. R. *J. Am. Chem. Soc.* **1996**, *118*, 10228–10235.
(21) Greenfield, S. R.; Svec, W. A.; Gosztola, D.; Wasielewski, M. R. *J. Am. Chem. Soc.* **1996**, *118*, 6767–6777.
(22) Gonen, O.; Levanon, H. *J. Phys. Chem.* **1985**, *89*, 1637–1643.
(23) *Handbook of Mathematical Functions, with Formulas, Graphs, and Mathematical Tables*; Abramowitz, M., Stegun, I. A., Eds.; Dover Publications: New York, 1965; p 600.

JP103678M